

Seafloor Electromagnetic Measurements above Axial Seamount, Juan de Fuca Ridge

S. C. CONSTABLE¹, G. S. HEINSON², G. ANDERSON¹, and A. WHITE²

¹*Scripps Institution of Oceanography, UCSD, La Jolla, CA 92093-0225, U.S.A.*

²*School of Earth Sciences, Flinders University, GPO Box 2100, Adelaide SA 5001, Australia*

(Received January 7, 1997; Revised July 25, 1997; Accepted September 12, 1997)

Magnetotelluric (MT) data were collected at three sites around the eastern rim of the caldera of Axial Seamount, on the Juan de Fuca Ridge. The seamount has been observed to be volcanically and hydrothermally active over the last ten years, and is therefore an excellent target for electromagnetic induction studies on the seafloor. This paper follows an initial interpretation by Heinson *et al.* (1996) with a more complete analysis of the MT data, to investigate both oceanographic induction effects and the resistivity structure beneath the seamount.

From time series analysis of electric field data using multitaper methods, coherences between electric field data from different sites are significant at the 95% confidence level at periods less than 1 day, and generally greater than 0.8 at solar and ocean tidal periods. Spectral peaks at 16.7 hours and 4 days are observed; the former is due to inertial currents in the area, and the latter is probably a ridge-trapped Rossby wave. Robust MT impedance tensors are derived using a remote-reference, and tensor decomposition shows that there is no galvanic distortion and almost isotropic responses at each site. The MT data are inverted for 1D structure, and more complex 3D forward models used to assess the lateral extent of the resistivity structure. 1D inversions show that the data are consistent with a crust with a very high electrical conductance of 1200 ± 200 S and an asthenosphere of 5–50 $\Omega\cdot\text{m}$ at a depth of 40 km, connected by a low resistivity lithosphere of 50–100 $\Omega\cdot\text{m}$. The low resistivity lithosphere acts as a leakage path to the mantle for induced currents in the ocean. 3D forward modelling suggests that this region may be present only beneath Axial Seamount, surrounded by a resistive lithosphere of 500–50,000 $\Omega\cdot\text{m}$. The tectonic implications from these models are that a small fraction of melt is presently migrating from the melt source in the mantle to a crustal magma chamber beneath Axial Seamount. Bulk estimates of melt fractions are 1–10% for the asthenosphere, and 1% between the asthenosphere and the crustal magma chamber, although melt may be concentrated in fractures or pipes.

1. Introduction

Axial Seamount lies on the Juan de Fuca Ridge, about 500 km west of the northwest American coastline. Although part of the mid-ocean ridge, its origin is also linked to the Cobb-Eickelberg Seamount Chain (Johnson and Embley, 1990). Basalts from Axial Seamount are broadly similar to those from the rest of the Juan de Fuca Ridge and there are none of the enriched (E-type) or alkali basalts characteristic of some seamounts. Geochemical evidence (Desonie and Duncan, 1990; Rhodes *et al.*, 1990) suggests that the Cobb hotspot is a stationary upper-mantle melting anomaly whose volcanic products show strong mid-ocean ridge basalt (MORB) affinity. The volcano is the shallowest part of the Juan de Fuca Ridge, indicating a significant and robust supply of magma (e.g., Delaney *et al.*, 1981). The summit of the volcano has a well-defined, three-sided caldera (e.g., Fox, 1990), as shown in Fig. 1, which has developed from the complex interaction of the seamount with the Vance and Cobb Segments of the Juan de Fuca Ridge (Embley *et al.*, 1990).

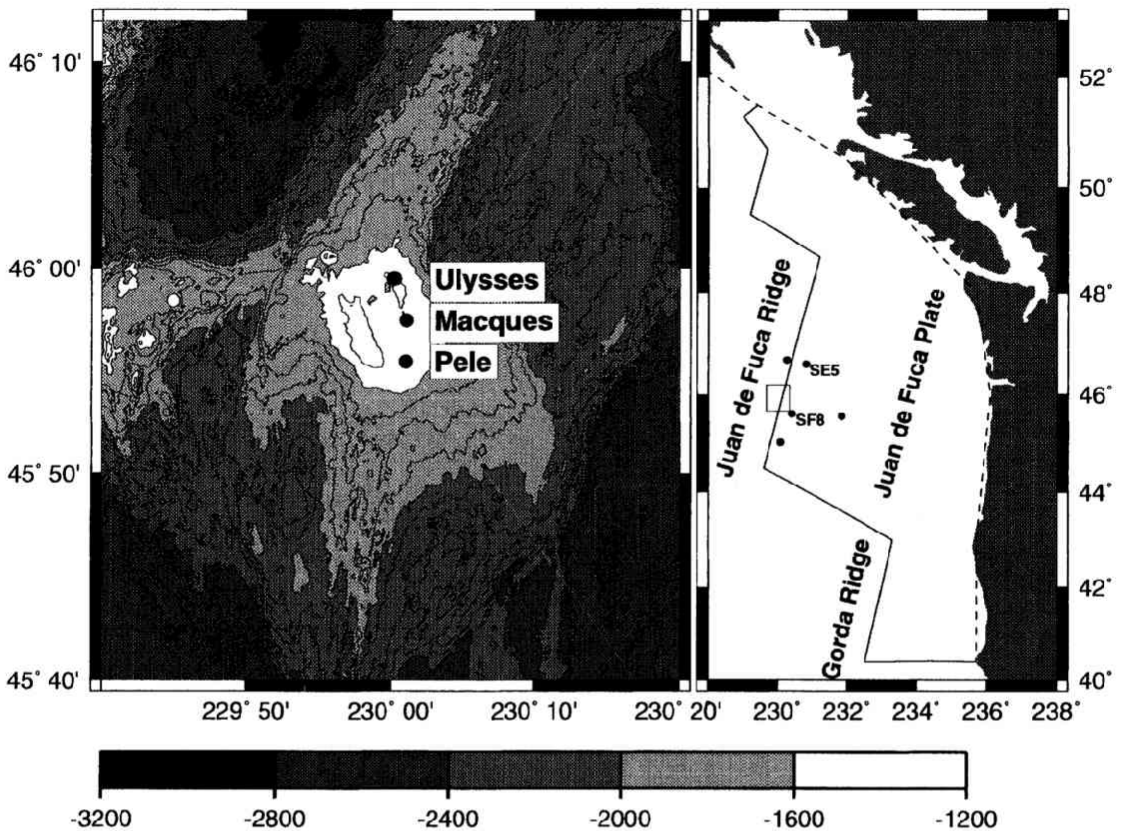


Fig. 1. Site location of Axial Seamount and the three MT instruments. The left hand figure is a contour map of the Seamount, with gray-scale interval of 400 m and contour interval of 100 m. Distance between adjacent sites is about 4 km. The white dashed lines approximately indicate the principal axes azimuths determined from MT impedance tensor decompositions. In the right hand figure, the major ridge and transform boundaries of the Juan de Fuca plate are shown by solid lines, and the dashed line delineates the subduction zone. The study area is shown by the box along the Juan de Fuca Ridge, and nearby EMSLAB MT sites are indicated by small circles.

Axial Seamount is currently volcanically and hydrothermally active. Very recent lava flows and low-level hydrothermal activity and deposits have been mapped using Sea Beam and Sea-MARC I swath bathymetry systems, coupled with towed cameras and submersible observations (Embley *et al.*, 1990). Fox (1990), using a precision pressure sensor, measured an abrupt 15 cm movement of the caldera floor, associated with deflation of the caldera and a related thermal plume. Elongated rifts to the north and south of the volcano summit show evidence of along-strike, near-surface magma transport (Appelgate, 1990; Embley *et al.*, 1990). There is limited geophysical evidence for a crustal magma chamber. Modelling of sea-surface magnetic data (Tivey and Johnson, 1990) and gravity data (Hildebrand *et al.*, 1990) are consistent with a high temperature/low density body at a depth of a few km, but the interpretations were non-unique.

During July to September 1994, we deployed a variety of geophysical instrumentation on Axial Seamount, primarily as part of a test of seafloor tiltmeters (Anderson *et al.*, 1997). The location of the experiment was to some extent driven by the detection of a large earthquake swarm at Axial Seamount a week before the deployment, using the US Navy's acoustic listening

arrays (SOSUS). The instruments deployed were 6 ocean-bottom seismometers/short-baseline tiltmeters, 4 long-baseline two-fluid tiltmeters, and the 3 magnetotelluric recorders. Deployment of the MT equipment on this experiment was motivated by the hope that variations in either the local magnetic field or the magnetotelluric response would accompany pre-eruptive migration of magma. Thus, the MT array was designed to observe temporal variations in the fields and less suited to structural studies. Earthquake activity abated as soon as our experiment started and no significant variations were detected in either the background magnetic field or the MT responses. However, the MT response was significantly different from those previously observed near ridge systems. Heinson *et al.* (1996) presented an initial interpretation of MT data collected from the summit of Axial Seamount. The MT responses were shown to be consistent with a crust of resistivity 1–5 $\Omega\cdot\text{m}$, and an asthenosphere at 30 km below the seafloor of resistivity 10 $\Omega\cdot\text{m}$, separated by a 20–100 $\Omega\cdot\text{m}$ depleted mantle. The sub-structure could be interpreted as 1D, and the small anisotropy in apparent resistivity was primarily due to seafloor topography. This paper reports a more extensive analysis of the data, for oceanographic induced effects and the MT response of the resistivity structure beneath the seamount. In particular, 3D modelling of the seamount is used to assess the lateral extent of resistivity structure required by the data to quantify the importance of Axial Seamount as a leakage path linking a magmatically active crust to partial melt in the asthenosphere.

2. Instrumentation and Data

Three sets of MT instruments were deployed from 3rd July to the 7th September, 1994 from the Oregon State University Research Vessel *Wecoma*. The GPS-determined deployment locations and depths (Fig. 1) were for Pele: 45° 55.47' N, 129° 59.03' W (1550 m), Macques: 45° 57.48' N, 129° 58.98' W (1520 m) and Ulysses: 45° 59.50' N, 129° 59.81' W (1490 m).

Magnetotelluric recorders were created by installing the ring-core fluxgate instruments of White (1979) into the electrometer described by Constable and Cox (1996), which features two orthogonal arms 10 m long terminated by silver-silver chloride electrodes. Water chopping (Filloux, 1987) was not used to remove electrode drift, but this appears only necessary to study the longest period oceanographic signals. For MT work it is adequate to use a smoothing spline to remove the smooth and monotonic drift (see below).

Magnetometer data were corrected for tilt and clock drift, and had a few jumps and spikes removed using cubic-spline interpolation. Electrometer data were averaged into 30 s values to match the magnetometer sampling rate and required only a minor interpolation to remove a spike at the beginning of the data block of 4096 records caused by operating the disk drive. Figure 2 shows a one-day example (2880 points, day 195 is 14th July) of five-component data from Macques in the original instrument orientation. The data have an arbitrary baseline subtracted from the original records for the purpose of plotting, so the y -axis scale is in relative units. There is clear coherence at all periods at this plotting scale between the electric and magnetic field components B_x and E_y , and B_y and E_x , as would be expected. The Z field is very smooth, particularly at periods less than a few hours, suggesting that there are no major lateral variations in electrical conductivity in close proximity to Macques.

3. Motionally Induced Signals

The movement of seawater through the geomagnetic field generates electric currents through the Lorentz force ($\mathbf{E} = \mathbf{v} \times \mathbf{B}$). At periods longer than that of the semi-diurnal M_2 tide (12.4 hours), barotropic ocean motions are the largest source of electric fields measured on the seafloor (Filloux, 1987). A best-fit depleted-basis B-spline (Constable and Parker, 1988) was subtracted from all electrometer records to eliminate low-frequency drift due to long-term instrument settling.

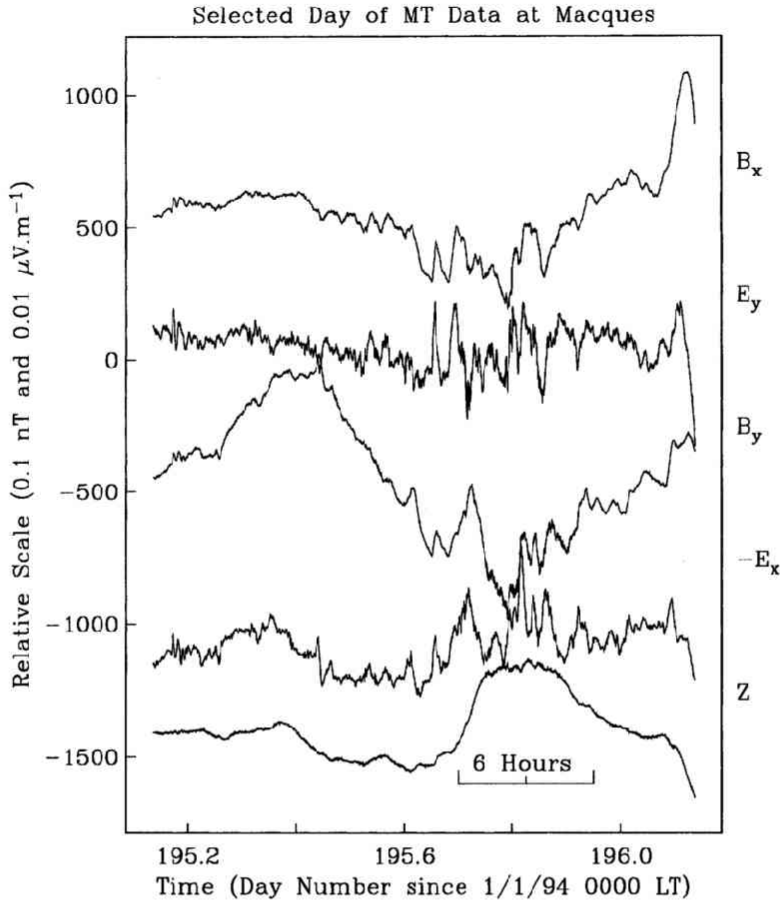


Fig. 2. A one-day example (2880 points, day 195 is 14th July) of five-component data from Macques in the original instrument orientation. The baselines for the data are arbitrary and show relative deviations.

All six residual electric field records display very similar tidal signatures with typical amplitudes of about $\pm 3 \mu\text{V m}^{-1}$, which can be converted to current speeds of 5–10 cm s^{-1} .

Cross-platform coherence estimates and empirically-determined 95% significance levels were computed using multitaper methods (Park *et al.*, 1987; Vernon *et al.*, 1991) and the method of Anderson *et al.* (1997), respectively. At frequencies greater than 1 cpd, coherences are generally significant at the 95% level, and are greater than 0.8 at the ocean tidal and solar daily variation periods of 1, 2 and 3 cpd. Multitaper cross-spectral estimates indicate zero relative phase between the records from different electrometers, suggesting that all instruments recorded the same signals.

Figures 3(a)–(c) show multitaper power spectral estimates of the electric field data, with spectral units converted from $(\mu\text{V m}^{-1})^2 \text{cpd}^{-1}$ to $(\text{cm s}^{-1})^2 \text{cpd}^{-1}$ assuming barotropic currents and a vertical magnetic field of 55,000 nT. Major peaks are evident at frequencies of 1, 2, 3, and 4 cpd, a small peak occurs at about 1.5 cpd, and a broad peak centered at 0.25 cpd is also apparent in the spectra from Macques and Pele. Peaks centered at 1, 2, 3, and 4 cpd are due to a mixture of ocean tides and solar daily variation and their harmonics (Filloux, 1987; Chave *et al.*, 1989), while the peak at 1.5 cpd corresponds to inertial motions due to the interaction of wind-driven currents and the Coriolis force.

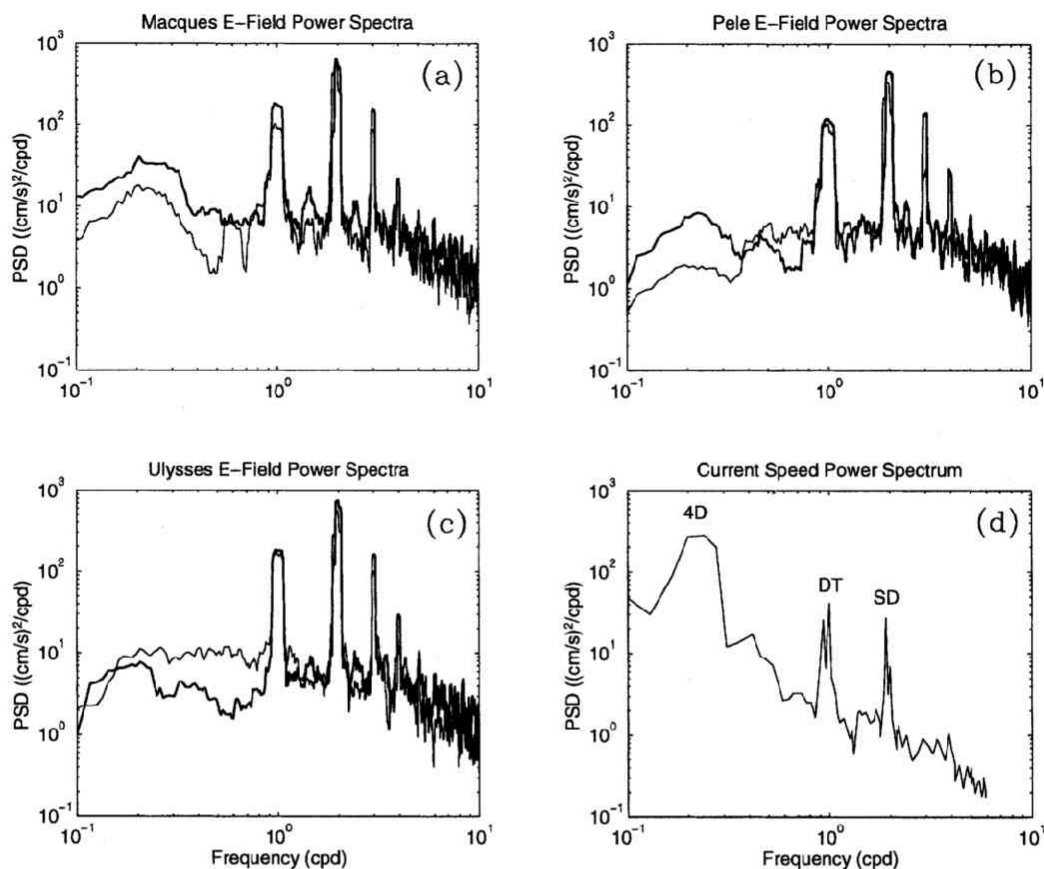


Fig. 3. (a)–(c) Power spectra from Macques, Pele, and Ulysses converted to ocean current speed. Geomagnetic north components are shown by the thick lines, geomagnetic east components by thin lines. Note strong peaks at 1, 2, 3 and 4 cpd due to solar and ocean tides and their harmonics, a smaller peak at 1.5 cpd which is the inertial frequency, and a broad peak centered at 0.25 cpd. (d) Power spectrum of current meter data collected near Axial Seamount by Cannon and Pashinski (1990). Peaks at 0.25 cpd and the frequencies of the diurnal and semi-diurnal tides are denoted 4D, DT and SD respectively.

The broad peak centered at 0.25 cpd frequency (4 day period) is the most interesting to oceanographers, as it is probably due to a topographically-trapped Rossby wave along the Juan de Fuca Ridge (Cannon and Thomson, 1996); similar observations were made during the EMSLAB experiment (Chave *et al.*, 1989) and by Cannon and Pashinski (1990). The spectrum shown in Fig. 3(d) was computed from current meter data collected near Axial Seamount (Cannon and Pashinski, 1990) and generally agrees with our electric field spectra. Observations of ridge-trapped waves are fairly rare in the literature (see the review by Luther, 1995), and therefore our observation is significant.

4. Magnetotelluric Response Estimation

The robust, remote-reference algorithm of Chave and Thomson (1989) was used to obtain impedance estimates in the period bandwidth 10^2 to 10^5 s. Magnetic data from the Victoria Magnetic Observatory (VMO) were used as a remote-reference. Leverage effects, due to auroral

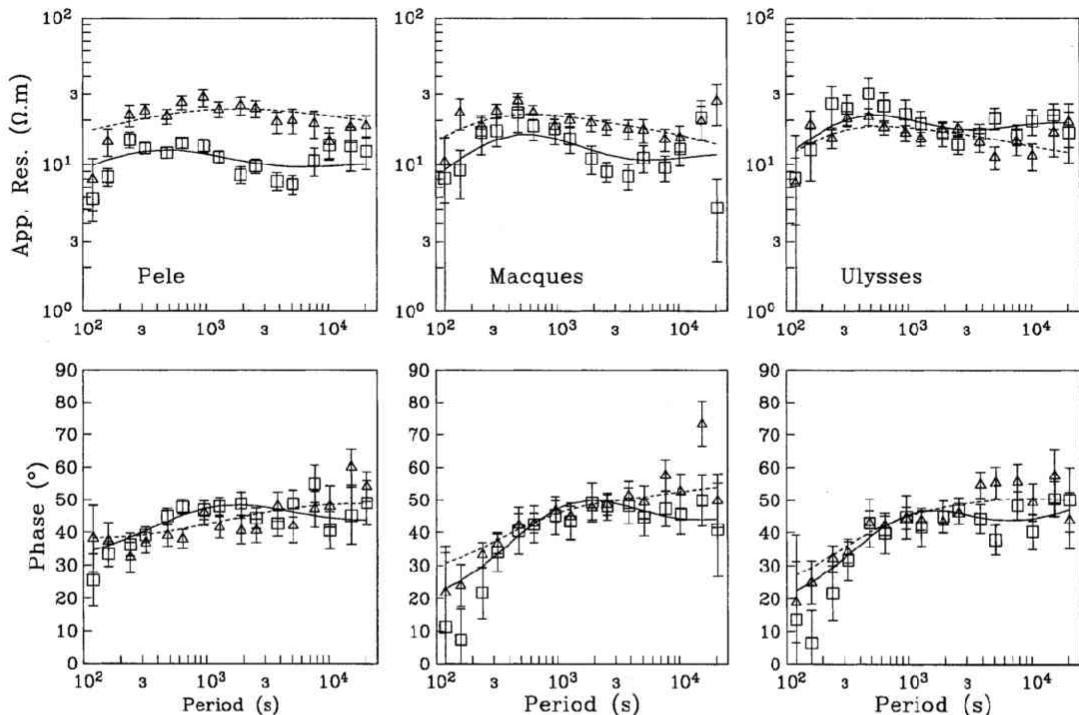


Fig. 4. Observed MT responses with one standard deviation error estimates for the three MT sites above Axial Seamount. The square symbols show MT estimates in the geographic north-south orientation, while triangle symbols are for geographic east-west. Solid and dashed lines indicate the model responses from the 1D inversions in Fig. 6.

activities, were automatically removed in the processing. For sites Pele and Macques, five components of magnetic and electric field were recorded for at least fourteen days, but at site Ulysses, only a few days of magnetic data were recorded. For the analysis that follows, MT responses for Ulysses were determined using electric field data from that site and magnetic field data from Macques.

Figure 4 shows apparent resistivities and phases (with one standard deviation errors) in geographic coordinates for all sites. The main features of the MT responses were discussed by Heinson *et al.* (1996). However, it is worth noting that the east-west apparent resistivities ρ_{yx} are larger than the north-south apparent resistivities ρ_{xy} , but are all between 5–25 $\Omega\cdot\text{m}$. Phases are similar, with less than 10° difference between orthogonal modes at all periods, and increase from 10° to 40 – 50° at periods longer than 1,000 s. The relatively isotropic response above Axial Seamount is unexpected given the proximity of the North American coast and the anisotropy observed in the EMSLAB responses (Wannamaker *et al.*, 1989a). Off-diagonal elements of the impedance tensors are smaller than diagonal elements, but are not zero. The magnitudes of impedance elements Z_{yy} are about an order of magnitude smaller than the diagonal elements, and Z_{xx} about two orders of magnitude smaller.

Tensor decomposition, using the methods described by Groom and Bailey (1989) and Chave and Smith (1994), was carried out to assess the importance of galvanic and magnetic distortion in the MT responses. Jackknife error estimates were obtained for the decomposed tensor impedances (Chave and Thomson, 1989; Thomson and Chave, 1991). Figure 5(a)–(c) shows the

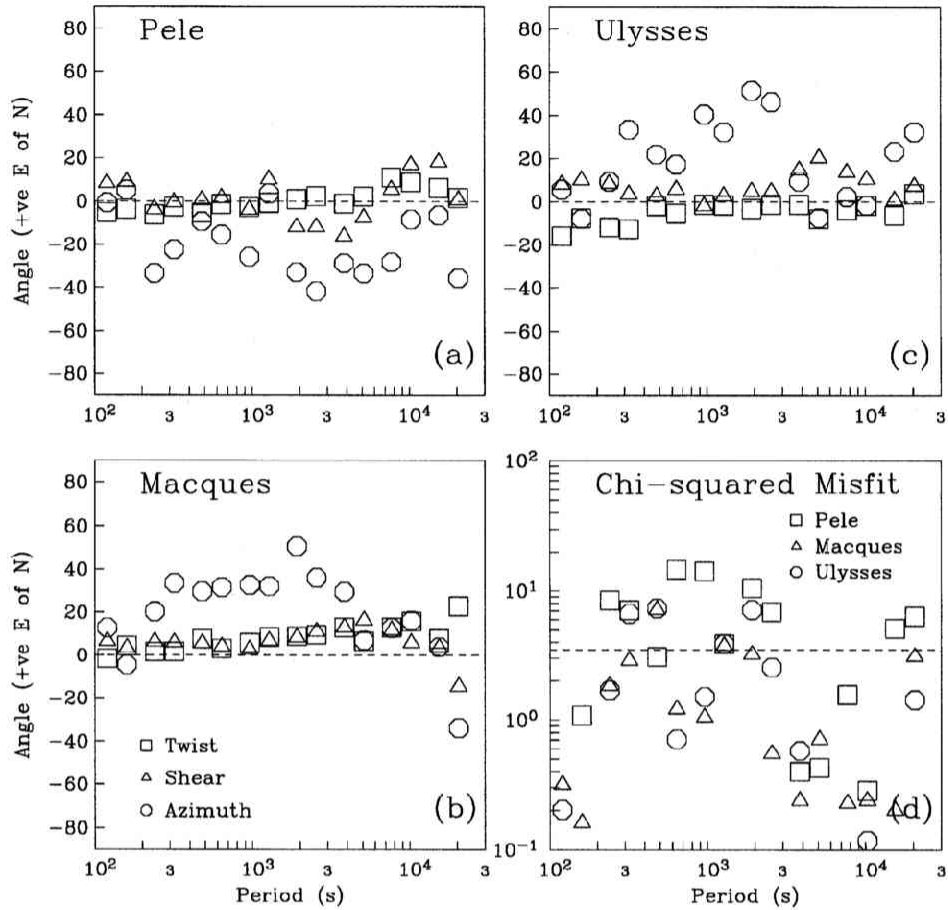


Fig. 5. (a)–(c) Twist, shear and regional azimuth parameters for a frequency-by-frequency electric field galvanic distortion model fit to the MT data at the three sites. The azimuth is positive east of geographic north, while the twist and shear are positive east of the regional strike. (d) The χ^2 misfits for a frequency-by-frequency electric field galvanic distortion model of each site. Sites Ulysses and Macques are below the 95% confidence limit (dashed line) at almost all periods, whereas the fit to Pele is slightly higher.

twist, shear and azimuth determined in a frequency-by-frequency galvanic decomposition for the MT data; azimuths are also shown in Fig. 1 at each site. Twist and shear angles are approximately frequency-independent, and are generally less than 10°, indicating that distortion is weak. The azimuth for Macques up to 4,000 s is about 35° east of geographic north, at longer periods it is not so well constrained. At short periods, the azimuth shows the influence of the deeper ocean to the northeast of the site (as shown in Fig. 1), but at long periods the coast effect is more significant and the azimuth is aligned with the coast which is approximately north-south. A similar change was noted for EMSLAB data by Chave and Smith (1994). For Pele, the azimuth is less well constrained, between 20 and about 40° west of geographic north (showing the influence of the deeper ocean to the southeast of the site in Fig. 1), and for Ulysses there is almost no consistent azimuth, indicating that the data are close to being 1D.

Chi-squared (χ^2) misfits between the predicted impedances from the model of galvanic distortion and observed impedances are also shown in Fig. 5(d). Chave and Smith (1994) carefully

discuss the statistical significance of χ^2 in this context; we note from their work that for galvanic decomposition over broad period-bands, the 95% level is 3.5. χ^2 misfits for Macques and Ulysses are generally less than the 95% confidence level, while misfits for Pele are slightly larger, but still close to the 95% level. The model fits show that Axial Seamount MT responses are subject to galvanic distortion, but as twist, shear and splitting operators are much less than unity, the distortion is weak.

5. Electrical Resistivity Structure

Heinson *et al.* (1996) presented 1D and 2D inversions of the MT responses at Pele, using the Occam algorithms of Constable *et al.* (1987) and deGroot-Hedlin and Constable (1990). Here, we show further 1D inversions from all sites using the impedances after tensor decomposition to determine the principal resistivity structural features, and 3D modelling to examine lateral bounds on crust and mantle features and to assess the sensitivity of the MT data to the structure.

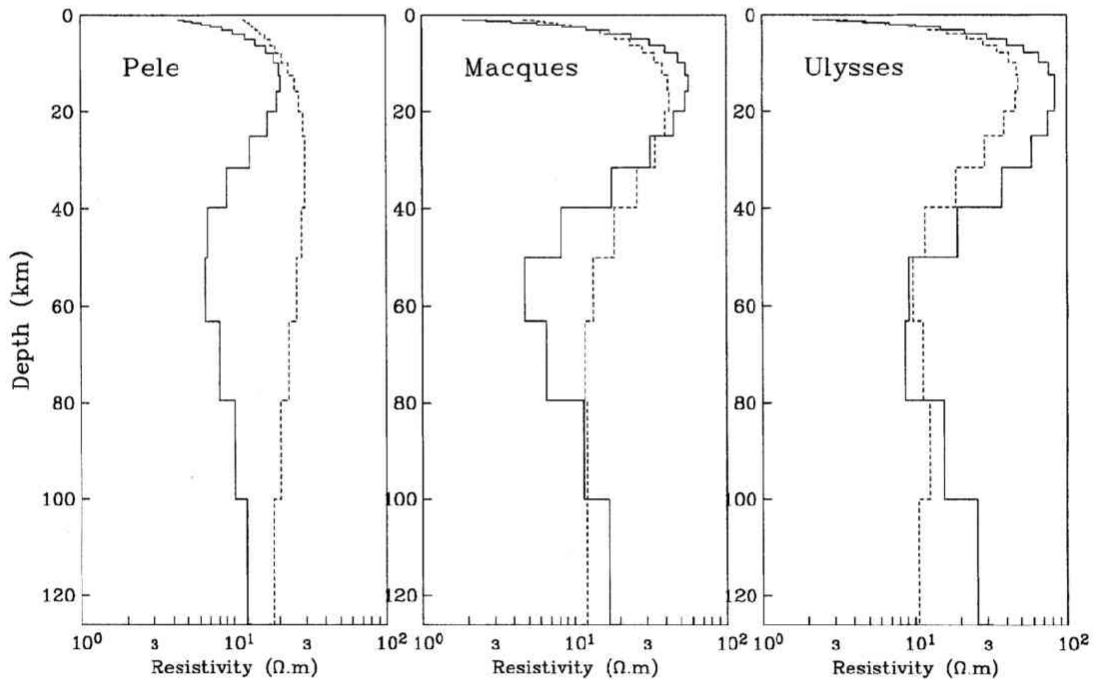


Fig. 6. 1D smooth Occam's inversions for Pele, Macques and Ulysses. The solid lines show the model for MT data in a geographic north-south orientation, the dashed lines are for the orthogonal components. Corresponding model fits to the data are shown in Fig. 4.

The azimuths of principal strike are only weakly constrained by the decomposition, and are inconsistent between sites only a few km apart. From the 2D inversions of Heinson *et al.* (1996), the small anisotropy in apparent resistivities at Pele are due primarily to the local-scale topography of the seamount, and similar arguments apply for Macques and Ulysses. We therefore have not rotated the impedance tensors to a new coordinate frame as there is no compelling evidence for 2D structure in the crust and mantle. Figure 6 shows the 1D Occam's inversions of

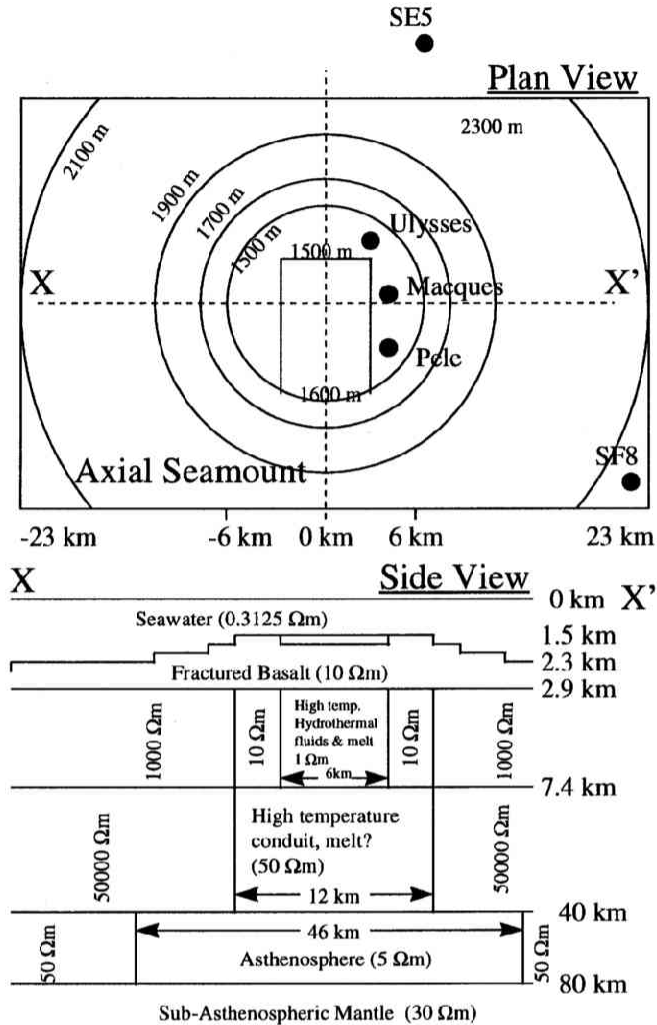


Fig. 7. A 3D model of Axial Seamount resistivity structure. Sites P, M and U represent the positions best approximating Pele, Macques and Ulysses. Approximate location of EMSLAB sites SF8 and SE5 are also indicated.

the data in MT data in geographic orientations, and the model fits to the data are given in Fig. 5. The minimum root mean squared (RMS) misfits from the D^+ method of Parker and Whaler (1981) were between 0.7 and 0.9 for each site in both induction modes. Occam's inversions in Fig. 6 are for an RMS misfit which is 25% larger than the D^+ minimum.

All inversions show the same features. Firstly, there is a low resistivity zone of 1–5 $\Omega\cdot\text{m}$ in the crust over the top few km. Structure within the crust is not resolved, however the bulk electrical parameter of conductance (vertically integrated conductivity) is robust to the model fit. The conductances for the three sites are in excellent agreement, at 1200 ± 200 S. This value is larger than the 800 S determined for an axial volcanic ridge segment at the Reykjanes Ridge (Heinson *et al.*, 1997) at which a magma chamber was imaged by both seismic and controlled source electromagnetic methods (Sinha *et al.*, 1997).

Beneath the Moho is a slightly more resistive layer of 50–100 $\Omega\cdot\text{m}$ to a depth of 40 km, a

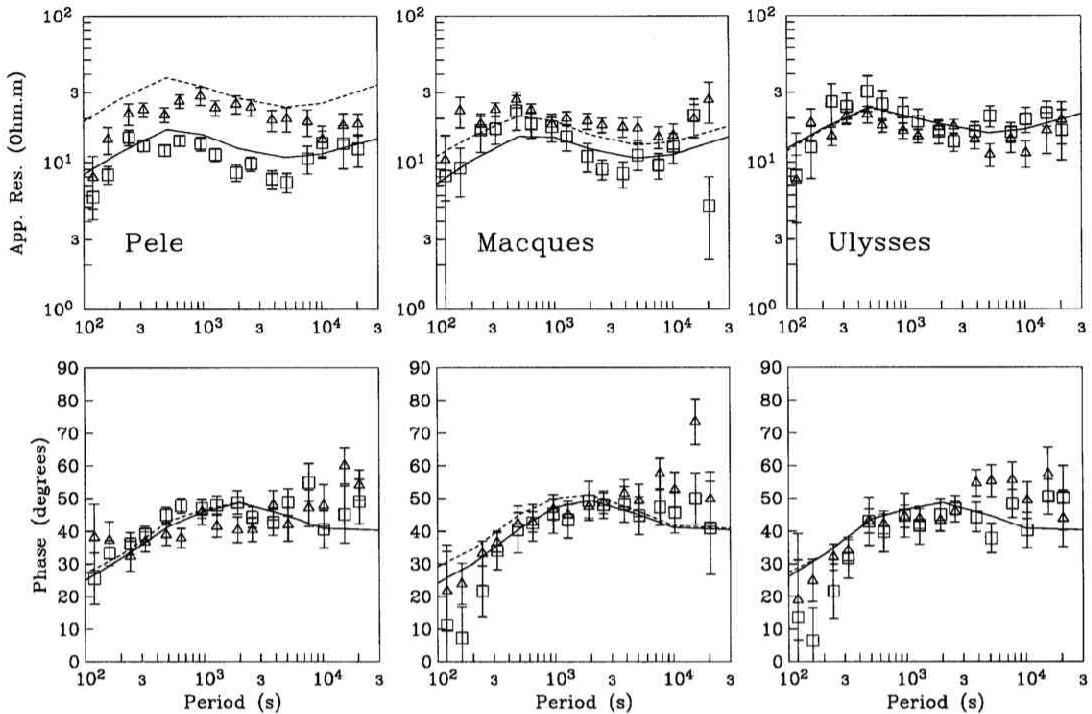


Fig. 8. The 3D modelled responses for the three MT sites. As for Fig. 4, data are in geographic coordinates.

low resistivity asthenosphere between 40 and 80 km of about $5\text{--}10\ \Omega\cdot\text{m}$, and a fall in resistivity to about $30\ \Omega\cdot\text{m}$ below 80 km. The resistivity at depths of a few hundred kilometers terminates at between $1\text{--}5\ \Omega\cdot\text{m}$, but this is only marginally resolved by the data. Inversions of the MT data in the west-east orientation show less structure than the orthogonal mode, and for Pele there is no indication of an asthenosphere.

Axial Seamount is clearly not a 1D layered structure due to the 3D seafloor topography and possible 2D influences of the Juan de Fuca Ridge. Furthermore, the EMSLAB model of the Juan de Fuca Plate (Wannamaker *et al.*, 1989b) is much more resistive than the inversions in Fig. 6, implying that the low-resistivity structure beneath the seamount is limited in lateral extent. The seamount is significantly higher than adjacent ridge segments, so that the anomalous mantle melting source is probably restricted to a region directly below the seamount, unless efficient channeling of melt occurs along the Juan de Fuca Ridge.

A 3D model study was used to assess the effects of seafloor topography and the limited lateral extent of crust and mantle low-resistivity structures, using the method and algorithm of Mackie and Madden (1993a,b) and Mackie *et al.* (1993) adapted for seafloor MT. The 3D model, shown in Fig. 7, consists of a circular seamount with a three-sided caldera. The top of the seamount is at 1500 m depth, increasing to a maximum of 2300 m at a distance of 4 km from the summit. A 6.4-km-thick crust beneath the seamount comprises a 600 m layer of fractured basalts with resistivity $10\ \Omega\cdot\text{m}$ over 5.8 km of sheeted dykes and intrusives with lower porosity and resistivity $1,000\ \Omega\cdot\text{m}$. Embedded in the crust at a depth of 1.5 km is an approximately circular region of resistivity $2.5\ \Omega\cdot\text{m}$, diameter 8 km and thickness 3 km. This crustal low-resistivity region has a conductance of 1200 S to agree with the 1D inversions, and represents a magma chamber of low melt fraction and hydrothermal circulation. An upper mantle of resistivity $50,000\ \Omega\cdot\text{m}$ extends

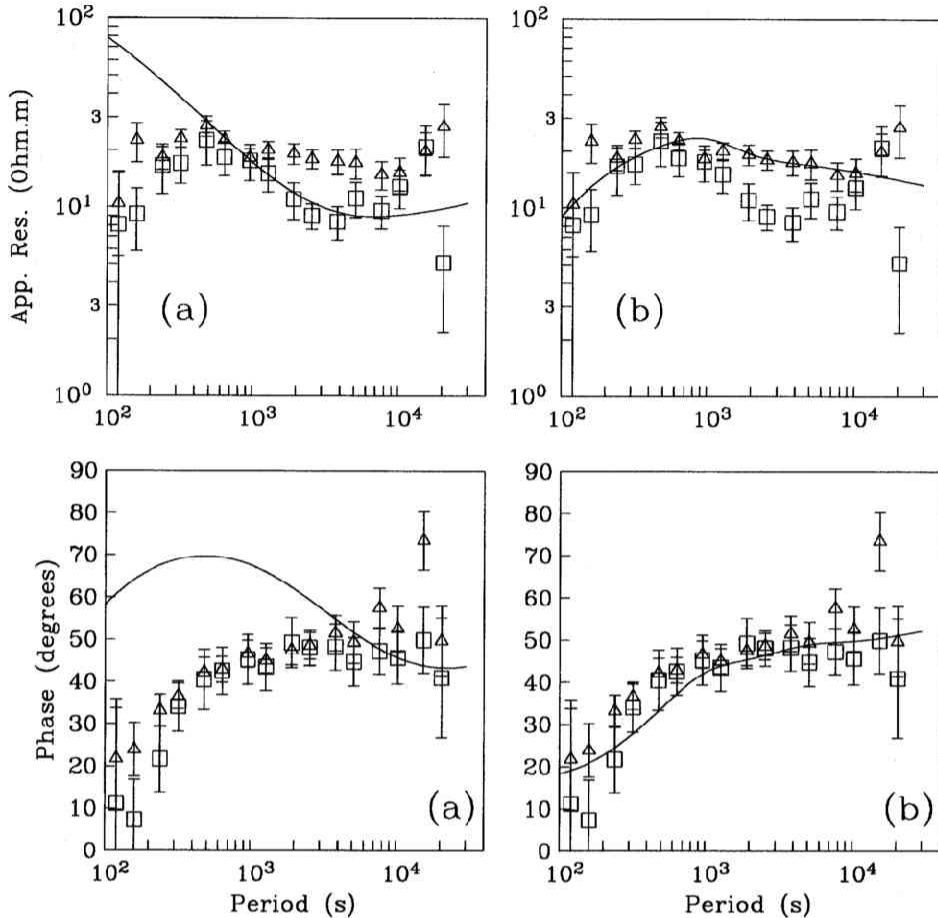


Fig. 9. The model response of the resistivity structure in Fig. 7 compared with MT data from Macques for the case in which (a) there is no crustal magma chamber and a uniform crustal structure of 10–1,000 $\Omega\cdot\text{m}$ exists, (b) the asthenosphere layer over depths of 40–80 km has resistivity of 50 $\Omega\cdot\text{m}$ instead of 5 $\Omega\cdot\text{m}$.

to 40 km depth, underlain by a 40-km-thick asthenosphere of 5 $\Omega\cdot\text{m}$. Beneath the asthenosphere, there is a uniform layer of 30 $\Omega\cdot\text{m}$ to 400 km depth and a terminating mantle resistivity of 10 $\Omega\cdot\text{m}$. The low-resistivity zone in the crust is connected to the asthenosphere by a 50 $\Omega\cdot\text{m}$ conduit of diameter 12 km. Resistivity structure away from the seamount is similar to that used for the EMSLAB model by Wannamaker *et al.* (1989b).

Figure 8 shows the modelled response at sites Macques, Pele and Ulysses in geographic coordinates. There is good agreement between modelled and observed data, including the anisotropy at site Pele which is principally due to variations in topography. In Fig. 9 two additional models are shown in comparison to observations at site Macques; one in which the crustal magma chamber is not present and the crust has a resistivity of 10 $\Omega\cdot\text{m}$ over the top 600 m and 1000 $\Omega\cdot\text{m}$ from 600 m to the Moho; and a second model in which the electrical asthenosphere over depths 40–80 km has resistivity 50 $\Omega\cdot\text{m}$. There is a degrading of the model fit by omitting either the magma chamber or asthenosphere. If the magma chamber is removed (Fig. 9(a)), apparent resistivities at the shortest periods are of the order of 100 $\Omega\cdot\text{m}$, a factor of ten larger than observed. Similarly, modelled phase angles are greater than 60°, whereas observed values are 10–20°. If the resistivity

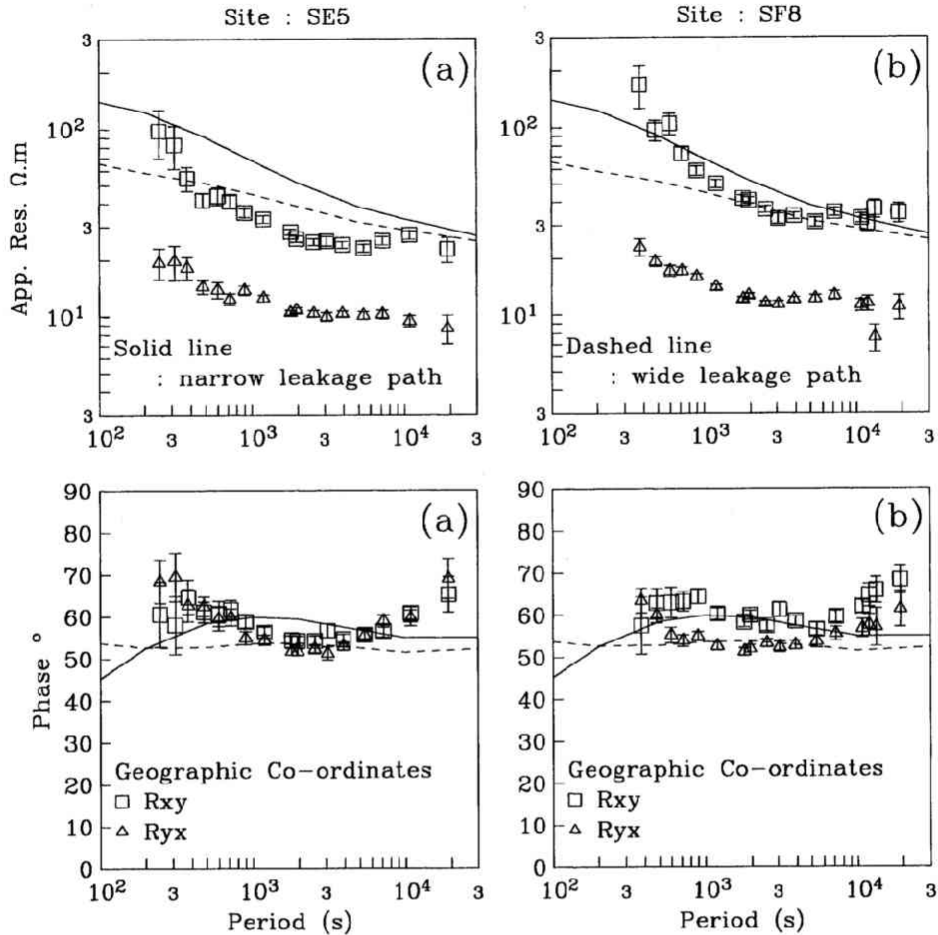


Fig. 10. MT data in geographic coordinates from EMSLAB sites SF8 and SE5 shown in Fig. 1. Superimposed are 3D model responses at the EMSLAB sites for the resistivity structure shown in Fig. 7. Two cases are shown, the first (a) has a narrow leakage path of $50 \Omega\text{-m}$ directly beneath Axial Seamount which is surrounded by a lithosphere of resistivity $50,000 \Omega\text{-m}$, and (b) where the lithosphere over the top 40 km all has a resistivity of $50 \Omega\text{-m}$.

of the asthenosphere is increased from 5 to $50 \Omega\text{-m}$, the fit to the data is not so bad, but the fall in resistivity in the TE mode between 1,000 and 10,000 s is not modelled. If asthenosphere resistivity is increased further to $100 \Omega\text{-m}$, the modelled response in apparent resistivity becomes much larger than observed.

Evidence for a low-resistivity leakage path beneath Axial Seamount is largely inferred from the lack of significant geomagnetic coast effect in the data and the low apparent resistivities over the entire bandwidth (Heinson *et al.*, 1996). By comparison, nearby EMSLAB sites (see Fig. 1) exhibit a clear coast effect, with anisotropy in apparent resistivity of half an order of magnitude and high apparent resistivities at short periods (Wannamaker *et al.*, 1989a). Figure 10 shows MT data from sites SF8 and SE5, which are the two closest sites to Axial Seamount in Fig. 1, in geographic coordinates. Also shown are MT responses calculated from the 3D model in Fig. 7 away from the seamount. Two sets of model curves were calculated, one for which the leakage path of $50 \Omega\text{-m}$ has a diameter of 12 km directly beneath Axial Seamount, the second in which

the leakage path exists across the whole model.

The EMSLAB R_{xy} data are well reproduced by the 3D model with a narrow leakage zone, but note that apparent resistivities are too high when the leakage zone is extended across the whole model. As we have not included the North American coastline in the 3D model of Fig. 7, we do not reproduce the observed anisotropy, in the R_{yx} components. The two EMSLAB sites shown are to the east and north of Axial Seamount, and as both have similar responses we concluded that leakage appears to be limited to a narrow region beneath Axial Seamount, and there no compelling evidence from these limited data that leakage occurs all along the Juan de Fuca Ridge.

6. Conclusions and Discussion

There is now well-established evidence (e.g., Cox *et al.*, 1986) that, in general, the oceanic lithosphere has a resistivity-thickness product of $10^9 \Omega \cdot \text{m}^2$, with an age dependent thickness of a few tens of km. Young oceanic lithosphere thus has a resistivity of the order $10^5 \Omega \cdot \text{m}$, which prevents electric currents induced in the ocean from flowing into the asthenosphere. For a uniformly resistive lithosphere across the ocean basins, the geomagnetic coast effect extends hundreds or even thousands of km, significantly distorting seafloor MT data (Heinson and Constable, 1992). Leakage paths allow induced electric currents to flow out of the ocean to the asthenosphere, reducing the geomagnetic coast effect and consequently distortion (Tarits *et al.*, 1993). Examples of leakage have previously been observed at subduction zones, where fluid-saturated sediments are subducted along the plate margin (Wannamaker *et al.*, 1989b). Mid-ocean ridges and hot-spots may also act as leakage paths, where mantle melt migrates from the asthenosphere to a crustal magma chamber. However, the few published examples of seafloor MT at mid-ocean ridges (Filloux, 1981; Heinson *et al.*, 1993, 1997; Sinha *et al.*, 1997) have not detected low-resistivity zones connecting the ocean to the asthenosphere.

From a limited deployment of MT instrumentation, evidence is found for a low-resistivity leakage path beneath Axial Seamount. The MT responses show no galvanic distortion, indicating an approximately isotropic sub-structure beneath the seamount. 1D inversions and 3D forward models of these data indicate that the crust has low resistivity (with a total electrical conductance of $1200 \pm 200 \text{ S}$), an asthenosphere of $5\text{--}50 \Omega \cdot \text{m}$ exists at a depth of 40 km below the seafloor, and a low-resistivity zone of $50 \Omega \cdot \text{m}$ between crust and asthenosphere is present.

The crustal conductance is 50% higher than the 800 S determined for an axial volcanic ridge segment at the Reykjanes Ridge (Heinson *et al.*, 1997) where a magma chamber was detected by a combination of seismic and controlled source electromagnetic soundings. Given the recent volcanism and hydrothermal activity at Axial Seamount, and additional geophysical evidence from gravity and magnetic studies, the presence of a magma chamber is probable. All three sites have similar MT responses, suggesting that the magma chamber is at least 8 km wide, but there are no constraints on the thickness and consequently melt fractions.

A mantle melt source comprising about 5–10% melt at a depth of 40 km would give rise to the resistivities of 3–10 $\Omega \cdot \text{m}$ determined from the 1D inversions. Such melt percentages are consistent with MORB geochemical and petrological studies which indicate that 10–15% of the sub-ridge mantle melts. The depth of the melt source is determined with a resolution of about $\pm 10 \text{ km}$, implying that melting occurs in the spinel peridotite stability field (20–65 km) (Elthon, 1989).

Between asthenosphere and crust, the leakage path is modelled with a resistivity of $50 \Omega \cdot \text{m}$. To obtain this resistivity, an average melt fraction of about 1% in the uppermost mantle is present, although the melt may be concentrated in fractures and pipes of dimensions less than a few metres wide in an otherwise sub-solidus mantle. High melt fractions in small fractures would migrate to the crustal magma chamber very rapidly. Alternatively, if the mantle is very

close to the mantle solidus temperature, small fractions of melt may be stable or slowly migrating over a wider region. The MT data do not constrain the width of the melting region, although a lower bound of 8 km is probable given the uniform MT response and size of Axial Seamount. 3D forward model studies suggest that the low resistivity zone may be an isolated feature beneath Axial Seamount, surrounded by a 40 km thick lithosphere of 5,000–50,000 Ω -m, consistent with the EMSLAB model of the Juan de Fuca plate. The low-resistivity zone acts as a leakage path for induced electric currents in the ocean which negates the coast effect at Axial Seamount to give approximately 1D isotropic responses with no galvanic distortion. However, the extent to which Axial Seamount may act as a short circuit to induced electric currents in the northeast Pacific Ocean is probably limited, and there was no evidence from the EMSLAB data for significant leakage effects along much of the Juan de Fuca Ridge (Wannamaker *et al.*, 1989a).

Long-period electric field data also give oceanographic information. Although the data were not chopped to give a zero baseline measurement, removing long-term drift from the records using harmonic splines shows strong signals at solar and ocean tidal periods and to a lesser extent at the inertial period. Of more interest is the 4-day peak in the spectra, probably due to topographically trapped Rossby waves along the Juan de Fuca Ridge. Due to the non-unique removal of drift, the strength of the 4-day signal cannot be determined, but as such observations are rare (Chave *et al.*, 1989), it is an important result.

Axial Seamount is an excellent laboratory for future MT measurements, due to its shallow depth, concentration of geophysical and geochemical sensors, and the proximity to US and Canadian west coast ports. There is evidence from geophysical and geological studies that a substantial magma chamber is hydrothermally and volcanically active, which makes it an ideal target. For example, deployment of instrumentation around the base of the seamount will significantly improve the lateral resolution of crust and mantle structure, and additional high-frequency MT (Constable *et al.*, 1997) measurements at the caldera may provide important constraints on the crustal structure.

We thank the captain and crew of the R/V *Wecoma* for their expert assistance in the deployment and recovery of all instruments in this experiment. G. Heinson was funded by a Queen Elizabeth II Fellowship from the Australian Research Council, and S. Constable received funding from the NSF under grant number OCE 92 00879. Magnetic Observatory data from Victoria, Canada were kindly supplied by the Canadian Geological Survey. A. D. Chave is kindly thanked for making available his robust remote-reference MT code, and R. L. Mackie is thanked for his 3D modelling code. Figures were drafted using PLOTXY, provided by R. L. Parker and GMT software of P. Wessel and W. Smith (Wessel and Smith, 1991). M. Unsworth and N. Palshin are thanked for their constructive review comments which have improved the paper considerably.

REFERENCES

- Anderson, G., S. C. Constable, H. Staudigel, and F. K. Wyatt, A seafloor long-baseline tiltmeter, *J. Geophys. Res.*, **102**, 20,269–20,285, 1997.
- Appelgate Jr., T. B., Volcanic and structural morphology of the south flank of Axial Volcano, Juan de Fuca Ridge: results from a SeaMARC I side scan sonar survey, *J. Geophys. Res.*, **95**, 12,765–12,783, 1990.
- Cannon, G. A. and D. J. Pashinski, Circulation near Axial Seamount, *J. Geophys. Res.*, **95**, 12,823–12,828, 1990.
- Cannon, G. A. and R. E. Thomson, Characteristics of 4-day oscillations trapped by the Juan de Fuca Ridge, *Geophys. Res. Lett.*, **23**, 1,613–1,616, 1996.
- Chave, A. D. and J. T. Smith, On electric and magnetic galvanic distortion tensor decompositions, *J. Geophys. Res.*, **99**, 4,669–4,682, 1994.
- Chave, A. D. and D. J. Thomson, Some comments on magnetotelluric response function estimation, *J. Geophys. Res.*, **94**, 14,215–14,225, 1989.
- Chave, A. D., J. H. Filloux, D. S. Luther, L. K. Law, and A. White, Observations of motional electromagnetic fields during EMSLAB, *J. Geophys. Res.*, **94**, 14,153–14,166, 1989.

- Constable, C. G. and R. L. Parker, Smoothing, splines and smoothing splines; their application in geomagnetism, *J. Comput. Phys.*, **78**, 493–508, 1988.
- Constable, S. C. and C. S. Cox, Marine controlled-source electromagnetic sounding II: The PEGASUS experiment, *J. Geophys. Res.*, **101**, 5,519–5,530, 1996.
- Constable, S. C., R. L. Parker, and C. G. Constable, Occam's inversion: a practical algorithm for generating smooth models from electromagnetic sounding data, *Geophysics*, **52**, 289–300, 1987.
- Constable, S. C., A. Orange, G. M. Hoversten, and H. F. Morrison, Marine magnetotellurics for petroleum exploration I. A seafloor instrument system, *Geophysics*, 1997 (in press).
- Cox, C. S., S. C. Constable, A. D. Chave, and S. C. Webb, Controlled source electromagnetic sounding of the oceanic lithosphere, *Nature*, **320**, 52–54, 1986.
- deGroot-Hedlin, C. and S. C. Constable, Occam's inversion to generate smooth, two-dimensional models from magnetotelluric data, *Geophysics*, **55**, 1,613–1,624, 1990.
- Delaney, J. R., H. P. Johnson, and J. L. Karsten, The Juan de Fuca Ridge-hot spot-propagating rift system: New tectonic, geochemical and magnetic data, *J. Geophys. Res.*, **86**, 11,747–11,750, 1981.
- Desonie, D. L. and R. A. Duncan, The Cobb-Eickelberg Seamount Chain: hotspot volcanism with mid-ocean ridge basalt affinity, *J. Geophys. Res.*, **95**, 12,697–12,711, 1990.
- Elthon, D., Pressure of origin of primary mid-ocean ridge basalts, in *Magmatism in the Ocean Basins*, edited by A. D. Saunders and M. J. Norry, pp. 125–136, Geological Soc. Spec. Pub., 1989.
- Embley, R. W., K. M. Murphy, and C. G. Fox, High-resolution studies of the summit of Axial Volcano, *J. Geophys. Res.*, **95**, 12,785–12,812, 1990.
- Filloux, J. H., Magnetotelluric exploration of the North Pacific: progress report and preliminary soundings near a spreading ridge, *Phys. Earth Planet. Int.*, **25**, 187–195, 1981.
- Filloux, J. H., Instrumentation and experimental methods for oceanic studies, in *Geomagnetism*, edited by J. A. Jacobs, pp. 143–248, Academic Press, London, 1987.
- Fox, C. G., Evidence of active ground deformation on the mid-ocean ridge: Axial Seamount, Juan de Fuca Ridge, April–June 1988, *J. Geophys. Res.*, **95**, 12,785–12,812, 1990.
- Groom, R. W. and R. C. Bailey, Decomposition of magnetotelluric impedance tensors in the presence of local three-dimensional galvanic distortion, *J. Geophys. Res.*, **94**, 1,913–1,925, 1989.
- Heinson, G. S. and S. C. Constable, The electrical conductivity of the oceanic upper mantle, *Geophys. J. Int.*, **110**, 159–179, 1992.
- Heinson, G. S., A. White, L. K. Law, Y. Hamano, H. Utada, J. Yukutake, J. Segawa, and H. Toh, EMRIDGE: the electromagnetic investigation of the Juan de Fuca Ridge, *Mar. Geophys. Res.*, **15**, 77–100, 1993.
- Heinson, G. S., S. C. Constable, and A. White, Seafloor magnetotelluric sounding above Axial Seamount, *Geophys. Res. Lett.*, **23**, 2,275–2,278, 1996.
- Heinson, G. S., A. White, and S. C. Constable, RAMESSES IV: Seafloor magnetotelluric sounding above a slow-spreading ridge, *Geophys. J. Int.*, 1997 (submitted).
- Hildebrand, J. A., J. M. Stevenson, P. T. C. Hammer, M. A. Zumberge, R. L. Parker, C. G. Fox, and P. J. Meis, A seafloor and sea surface gravity survey of Axial Volcano, *J. Geophys. Res.*, **95**, 12,751–12,763, 1990.
- Johnson, H. P. and R. W. Embley, Axial Seamount: an active ridge axis volcano on the central Juan de Fuca Ridge, *J. Geophys. Res.*, **95**, 12,689–12,696, 1990.
- Luther, D. S., Waves trapped to discrete topography: existence and implications, *Topographic effects in the ocean, proceedings, 'Aha Huliko'a Hawaiian Winter Workshop, University of Hawaii at Manoa, January 17–20, 1995*, edited by P. Muller and D. Henderson, pp. 43–56, School of Ocean and Earth Science and Technology, University of Hawaii, Honolulu, 1995.
- Mackie, R. L. and T. R. Madden, Three-dimensional magnetotelluric inversion using conjugate gradients, *Geophys. J. Int.*, **115**, 215–229, 1993a.
- Mackie, R. L. and T. R. Madden, Conjugate direction relaxation solutions for 3-D magnetotelluric modelling, *Geophysics*, **58**, 1,052–1,057, 1993b.
- Mackie, R. L., T. R. Madden, and P. E. Wannamaker, Three-dimensional magnetotelluric modelling using difference equations-theory and comparison to integral equation solutions, *Geophysics*, **58**, 215–226, 1993.
- Park, J., C. R. Lindberg, and F. L. Vernon, Multitaper spectral analysis of high-frequency seismograms, *J. Geophys. Res.*, **92**, 12,675–12,684, 1987.
- Parker, R. L. and K. A. Whaler, Numerical methods for establishing solutions to the inverse problem of electromagnetic induction, *J. Geophys. Res.*, **86**, 9,574–9,584, 1981.
- Rhodes, J. M., C. Morgan, and R. A. Liias, Geochemistry of Axial Seamount lavas: magmatic relationship between the Cobb hotspot and the Juan de Fuca Ridge, *J. Geophys. Res.*, **95**, 12,713–12,733, 1990.
- Sinha, M. C., D. A. Navin, L. M. MacGregor, S. C. Constable, C. Peirce, A. White, G. S. Heinson, and M. A. Inglis, Evidence for accumulated melt beneath the slow-spreading Mid-Atlantic Ridge, *Phil. Trans. R. Soc. Lond.*, **355**, 233–253, 1997.

- Tarits, P., A. D. Chave, and A. Schultz, Comment on "The electrical conductivity of the oceanic upper mantle", by G. Heinson and S. Constable, *Geophys. J. Int.*, **114**, 711-716, 1993.
- Thomson, D. J. and A. D. Chave, Jackknife error estimates for spectra, coherences, and transfer functions, in *Advances in Spectrum Analysis and Array Processing*, edited by S. Haykin, pp. 58-113, Prentice-Hall, Englewood Cliffs, N.J., 1991.
- Tivey, M. A. and H. P. Johnson, The magnetic structure of Axial Seamount, Juan de Fuca Ridge, *J. Geophys. Res.*, **95**, 12,735-12,750, 1990.
- Vernon, F. L., J. B. Fletcher, L. Carroll, A. D. Chave, and E. Sembera, Coherence of seismic body waves from local events as measured by a small-aperture array, *J. Geophys. Res.*, **96**, 11,981-11,996, 1991.
- Wannamaker, P. E., J. R. Booker, J. H. Filloux, A. G. Jones, G. R. Jiracek, A. D. Chave, P. Tarits, H. S. Waff, G. D. Egbert, C. T. Young, J. A. Stodt, M. Martinez, L. K. Law, T. Yukutake, J. Segawa, A. White, and A. W. Green Jr., Magnetotelluric observations across the Juan de Fuca subduction system in the EMSLAB project, *J. Geophys. Res.*, **94**, 14,111-14,125, 1989a.
- Wannamaker, P. E., J. R. Booker, A. G. Jones, A. D. Chave, J. H. Filloux, H. S. Waff, and L. K. Law, Resistivity cross section through the Juan de Fuca ridge subduction system and its tectonic implications, *J. Geophys. Res.*, **94**, 14,127-14,144, 1989b.
- Wessel, P. and W. H. F. Smith, Free software helps map and display data, *EOS, Trans. AGU*, **72**, 441, 1991.
- White, A., A seafloor magnetometer for the continental shelf, *Mar. Geophys. Res.*, **4**, 105-114, 1979.